Journal of Materials Chemistry C

PAPER

View Article Online
View Journal | View Issue

Cite this: J. Mater. Chem. C, 2014, 2, 5673

Benzothiazole derivatives containing different electron acceptors exhibiting totally different data-storage performances†

Zhe Su,[a] Hao Zhuang,[a] Haifeng Liu,[a] Hua Li,*[a] Qingfeng Xu,[a] Jianmei Lu*[ab] and Lihua Wang[b]

Received 11th October 2013
Accepted 8th May 2014

DOI: 10.1039/c3tc32008a

www.rsc.org/MaterialsC

Two small conjugated molecules **BTVCz–NO$_2$** and **BTVCz**, each incorporating an electron-donating carbazole group and a medium electron-withdrawing benzothiazole group, were both successfully designed and synthesized. Molecule **BTVCz–NO$_2$** is an A1–D–A2 structure while **BTVCz** is a single D–A structure. Both molecules were made into thin films by spin-coating. The two films differentiated over their optical, electrochemical and morphological properties. And the fabricated device with **BTVCz–NO$_2$** as an active material showed non-volatile ternary WORM data-storage behavior with its switching threshold voltages at −1.5 V and −2.5 V in tandom when an electrical field was applied, whereas its "counterpart" device with **BTVCz** as an active material exhibited volatile binary DRAM data-storage behavior with its switching threshold voltage at −1.3 V. Combined with theoretical calculation of each molecule, we conclude that different data-storage behaviors can be achieved by introducing different electron acceptors and that molecule **BTVCz–NO$_2$**, as an A1–D–A2 structure, is more likely to achieve ternary data-storage performance.

1. Introduction

Organic and polymeric materials are poised to revolutionize the field of data storage due to their low-cost, structural flexibility, and three dimensional stacking capability.[1–15] Over the last decade, it has been reported that sandwich-structured memory devices fabricated using polymeric materials can exhibit good electrically bi-stable behavior with an ON/OFF current ratio of 10^4 to 10^6.[16–28] Until quite recently, small molecules have also been widely investigated in memory devices because of their designable molecular structures, high purity and excellent batch-to-batch reproducibility in contrast to polymer counterparts.[29–36] In our previous study,[37–39] we studied a series of memory devices based on azo-containing small molecules, with the results showing that these devices exhibited excellent ternary data-storage performances and increased data storage density by a wide margin. On the other hand, the introduction of azo groups largely increases the content of nitrogen atoms, which may result in the formation of conductive metal filaments and has a side effect on the performances of devices.[40,41] Therefore, synthesis of molecules with fewer azo components has gained, and will continue to gain more attention from the scientific world. Furthermore, most of the molecules we synthesized belong to either single Donor–Acceptor (D–A) molecules or Donor–Acceptor1–Acceptor2 (D–A1–A2) molecules, while asymmetric Acceptor1–Donor–Acceptor2 (A1–D–A2) molecules have rarely been studied. Compared with single D–A molecules, A1–D–A2 molecules have one more electron acceptor, A2. And compared with D–A1–A2 molecules, it can also prevent the overlapping of traps caused by their neighboring spatial locations, and lead to a well-proportioned distribution of the electron withdrawing groups, thus facilitating the access towards multilevel data-storage performances.

Herein, two organic small molecules **BTVCz–NO$_2$** and **BTVCz** have been successfully designed and synthesized. Each molecule incorporates a carbazole group and a benzothiazole group linked with a carbon–carbon double bond. The carbazole moiety is a large conjugated planar structure and has been widely used as a good hole transport moiety. In this case, it acts as a donor (D).[42] And the benzothiazole group, a thermally stable and moderate electron-withdrawing moiety,[43] acts as an acceptor (A) in both molecules, which has rarely been studied in the area of data-storage. Hence, molecule **BTVCz** is a single D–A structure. Within the molecule **BTVCz–NO$_2$**, a nitro group, which can diminish the band gap for its strong electron-withdrawing substitution effect, is also attached to the backbone of

[a]College of Chemistry, Chemical Engineering and Materials Science, Collaborative Innovation Center of Suzhou Nano Science and Technology, Soochow University, Suzhou 215123, P. R. China. E-mail: lujm@suda.edu.cn; Fax: +86 512 65880367; Tel: +86 512 65880368

[b]State Key Laboratory of Treatments and Recycling for Organic Effluents by Adsorption in Petroleum and Chemical Industry, Suzhou 215123, P. R. China

† Electronic supplementary information (ESI) available: The compositions of the small molecules, TGA, retention characteristics of two devices, *I–V* curves of the **BTVCz** device at different intervals, and the stability test of **BTVCz–NO$_2$** and **BTVCz**. See DOI: 10.1039/c3tc32008a

the carbazole moiety, forming an A1–D–A2 structure. Moreover, both molecules can be fabricated into ITO/film/Al sandwiched devices by spin-coating. The two molecules exhibit completely different optical, electrochemical and morphological properties in their films. And the fabricated devices exhibit totally different data-storage performances. Therefore, we can achieve different data-storage behaviors by introducing different numbers of acceptors with different electron-withdrawing abilities. What is more, A1–D–A2 structures are more likely to achieve ternary data-storage performance. We hope this new design concept of multi-level data storage materials can provide guidance for future realization of more superior high-density data storage devices (HDDS).

2. Experimental section

2.1 Materials

Carbazole, fuming nitric acid, 1-bromohexane, 4-methyl-benzaldehyde, *N*-bromosuccinimide, sodium-*t*-butoxide, phosphorus oxychloride, 2-aminothiophenol, *N*,*N*-dimethylformide (DMF) and triethyl phosphite were purchased from commercial sources (TCI, Alfa Aesar, and Sigma-Aldrich). All solvents were purchased from Sinopharm Chemical Reagent Co., Ltd. All chemicals were used as received without further purification.

2.2 Preparation of molecules

The compounds **BTVCz–NO$_2$** and **BTVCz** were prepared as detailed in Scheme 1.

9-Hexyl-6-nitro-9*H*-carbazole-3-carbaldehyde (2). The nitration was performed by dropping a small excess of fuming nitric acid (0.5 mL, 12 mmol) dissolved in acetic acid (3 mL) into a cooled, stirred solution made of **1** (2.8 g, 10 mmol) and acetic acid (20 mL). After ten minutes of further stirring, water was added, the solid precipitate was collected and washed thoroughly with water, and recrystallized twice from acetic acid. The crude product was purified by silica gel column chromatography (ethyl acetate–petroleum ether, 1/10, v/v) to give **2** (1.9 g, 50%). ^{1}H NMR (400 MHz, $CDCl_3$) δ 10.14 (s, 1H), 9.08 (s, 1H), 8.67 (s, 1H), 8.44 (d, J = 8.5 Hz, 1H), 8.12 (d, J = 8.8 Hz, 1H), 7.58 (d, J = 8.3 Hz, 1H), 7.50 (d, J = 8.5 Hz, 1H), 4.40 (d, J = 6.9 Hz, 2H), 1.91–2.01 (m, 2H), 1.31–1.5 (m, 6H), 0.88 (d, J = 7.2 Hz, 3H). ^{13}C NMR (100 MHz, $CDCl_3$) δ 191.30, 145.18, 144.26, 141.63, 130.00, 128.24, 124.57, 122.97, 122.72, 122.45, 117.52, 110.13, 109.17, 44.02, 31.42, 28.91, 26.85, 22.48, 13.99.

2-*p*-Tolylbenzo[d]thiazole (5). A mixture of 4-methyl-benzaldehyde (6.0 g, 50 mmol), 2-aminothiophenol (7.5 g, 60 mmol), and DMSO (30 mL) was heated in an oil bath to 195 °C, held at that temperature for 2 h, and then poured into water. The separated solids were recrystallized from ethanol to give **5** (8.8 g, 78%). ^{1}H NMR (400 MHz, DMSO-d6) δ 8.13 (d, J = 8.0 Hz, 1H), 8.04 (d, J = 8.1 Hz, 1H), 7.99 (d, J = 8.0 Hz, 2H), 7.60 (t, J = 7.7 Hz, 1H), 7.51 (t, J = 7.6 Hz, 1H), 7.40 (d, J = 8.2 Hz, 2H), 4.55 (s, 2H). ^{13}C NMR (100 MHz, $CDCl_3$) δ 168.27, 154.15, 141.46, 134.95, 130.95, 129.74, 127.51, 126.27, 125.03, 123.06, 121.59, 21.55.

2-(4-(Bromomethyl)phenyl)benzo[d]thiazole (6). Compound **5** (4.5 g, 20 mmol) and *N*-bromosuccinimide (NBS) (3.6 g, 20 mmol) were dissolved in 80 mL of CCl_4. The solution was heated and refluxed at 75 °C for 4 h. The precipitated succinimide was filtered, and the solvent was evaporated from the solution. The remaining gray oil was recrystallized from ethanol to afford white crystalline powder of compound **6** (5.2 g, 86%). ^{1}H NMR (400 MHz, DMSO-d6) δ 8.13 (d, J = 8.0 Hz, 1H), 8.04 (d, J = 8.1 Hz, 1H), 7.99 (d, J = 8.0 Hz, 2H), 7.62 (t, J = 7.7 Hz, 1H), 7.53 (t, J = 7.6 Hz, 1H), 7.45 (d, J = 8.2 Hz, 2H), 4.55 (s, 2H). ^{13}C NMR (100 MHz, $CDCl_3$) δ 167.18, 154.11, 140.59, 135.09, 133.61, 129.73, 127.96, 126.46, 125.40, 123.34, 121.68, 32.64.

(*E*)-2-(4-(2-(9-Hexyl-6-nitro-9*H*-carbazol-3yl)vinyl)phenyl)-benz[d]thiazole (8). Compound **6** (0.60 g, 2 mmol) and triethyl phosphite (0.5 mL, 3.1 mmol) were heated to reflux at 185 °C for 3 h under stirring. The resulting clear brown oil was then distilled under reduced pressure. Excess triethyl phosphite was collected at 69 °C (1.5 mm Hg) and compound **2** (0.58 g, 1.8 mmol) in dry DMF (5 mL) was added dropwise. NaOEt was added and the mixture was heated to 60 °C for 2 h. The mixture was cooled and quenched with EtOH. All solvents were then removed under reduced pressure. Solids were dissolved in

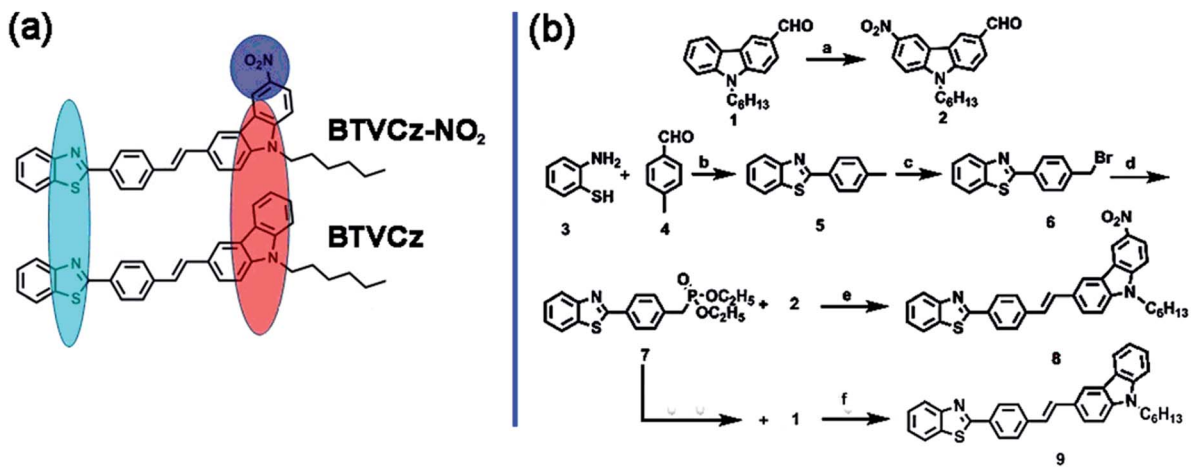

Scheme 1 (a) Chemical structure of BTVCz–NO$_2$ and BTVCz. (b) Synthesis routes to BTVCz–NO$_2$ and BTVCz.

CH_2Cl_2, washed with distilled H_2O, dried over $MgSO_4$ and the solvent was removed. The residue was chromatographed on a silica gel column (petroleum ether–dichloromethane, 2/1, v/v) to afford compound **8** (0.62 g, orange powder, 65%). m.p. 232.9–233.4 °C. ^{1}H NMR (400 MHz, $CDCl_3$) δ 9.09 (s, 1H), 8.43 (d, J = 9.1 Hz, 1H), 8.38 (s, 1H), 8.03–8.08 (m, 4H), 7.81–7.84 (m, 4H), 7.76 (t, J = 7.6 Hz, 1H), 7.61 (d, J = 16.2 Hz, 1H), 7.53 (d, J = 8.5 Hz, 1H), 7.47 (d, J = 9.2 Hz, 1H), 7.29 (d, J = 16.2 Hz, 1H), 4.39 (t, J = 6.9 Hz, 2H), 1.87–2.01 (m, 2H), 1.32–1.51 (m, 6H), 0.88 (d, J = 7.2 Hz, 3H). ^{13}C NMR (150 MHz, $CDCl_3$) δ 167.71, 154.29, 143.92, 141.49, 140.97, 140.21, 134.95, 132.22, 130.43, 130.03, 127.95, 127.73, 126.83, 126.46, 126.36, 126.25, 125.15, 123.33, 123.12, 121.85, 121.61, 119.29, 117.46, 110.00, 108.52, 43.79, 31.46, 28.94, 26.89, 22.50, 13.97. HRMS: calcd for $C_{33}H_{29}N_3O_2S$ $[M + H]^+$ 532.1980, found 532.2073.

(*E*)-2-(4-(2-(9-Hexyl-9*H*-carbazol-3yl)vinyl)phenyl)-benz[*d*]-thiazole (9). Compound **6** (0.60 g, 2 mmol) and triethyl phosphite (0.5 mL, 3.1 mmol) were heated to reflux at 185 °C for 3 h under stirring. The resulting clear brown oil was then distilled under reduced pressure. Excess triethyl phosphite was collected at 69 °C (1.5 mm Hg) and compound **1** (0.50 g, 1.8 mmol) in dry DMF (5 mL) was added dropwise. NaOEt was added and the mixture was heated to 60 °C for 2 h. The mixture was cooled and quenched with EtOH. All solvents were then removed under reduced pressure. Solids were dissolved in CH_2Cl_2, washed with distilled H_2O, dried over $MgSO_4$ and the solvent was removed. The residue was chromatographed on a silica gel column (petroleum ether–dichloromethane, 2/1, v/v) to afford compound **9** (0.66 g, yellow powder, 75%). m.p. 181.8–182.6 °C. ^{1}H NMR (400 MHz, $CDCl_3$) δ 8.36 (d, J = 7.6 Hz, 1H), 8.26 (s, 1H), 8.11–8.14 (m, 4H), 8.00 (d, J = 8.0 Hz, 1H), 7.92 (d, J = 7.9 Hz, 1H), 7.80 (d, J = 8.6 Hz, 1H), 7.68 (d, J = 8.2 Hz, 1H), 7.52–7.40 (m, 5H), 7.32 (d, J = 16.2 Hz, 1H), 7.23 (d, J = 16.7 Hz, 1H), 4.34 (t, J = 6.9 Hz, 2H), 1.87–2.01 (m, 2H), 1.37–1.48 (m, 6H), 0.88 (d, J = 7.2 Hz, 3H). ^{13}C NMR (150 MHz, $CDCl_3$) δ 167.93, 154.09, 140.85, 140.49, 134.90, 131.79, 131.51, 128.00, 126.63, 126.34, 125.90, 125.09, 124.84, 124.58, 123.22, 123.03, 122.81, 121.59, 120.44, 119.11, 119.06, 108.97, 108.92, 43.23, 31.57, 28.98, 26.97, 22.55, 14.03. HRMS: calcd for $C_{33}H_{30}N_2S$ $[M + H]^+$ 486.2130, found 486.2167.

2.3 Measurements

^{1}H NMR and ^{13}C NMR spectra were obtained on an Inova 400 MHz FT-NMR spectrometer. UV-vis absorption spectra were recorded using a Perkin-Elmer Lambda-17 spectrophotometer at room temperature. SEM images were captured on a Hitachi S-4700 scanning electron microscope. IR spectra were obtained on a Nicolet iS10 FT-IR spectrometer. X-ray diffraction (XRD) analysis was performed on films using a Shimadzu XRD-6000 spectrometer with a Cu KR monochromatic radiation source at 40 kV and 30 mA. The 2θ angle was scanned from 5° to 30°.

2.4 Fabrication of memory device

The memory devices consisting of films of organic molecules sandwiched between an indium-tin-oxide (ITO) bottom electrode and an Al top electrode were fabricated. The cyclohexanone solution of two molecules (10 mg mL^{-1}) was spin-coated (2000 r s^{-1}, 40 s) onto ITO and the solvent was removed in a vacuum chamber at 60 °C for 12 h. The film thickness was about 80 nm. Finally, a layer of Al was thermally evaporated and deposited onto the organic surface at about 5×10^{-4} Pa through a shadow mask to form the top electrode and so as to define an active cross-sectional area of 0.0314 mm^2 (a nummular point with a radius of 0.1 mm). All electrical measurements of the device were characterized under ambient conditions, without any encapsulation, using a HP 4145B semiconductor parameter analyzer.

3 Results and discussion

3.1 Thermal properties

The thermal stabilities of **BTVCz–NO$_2$** and **BTVCz** were evaluated by TGA under a nitrogen atmosphere at a heating rate of 10 °C min^{-1}. It showed (Fig. S1, ESI†) that the temperature for 5% weight loss of **BTVCz–NO$_2$** in nitrogen was up to 220 °C, while that of **BTVCz** was 210 °C, demonstrating the good thermal stability of the materials.

3.2 Current–voltage (*I–V*) characteristics

A schematic sandwich structure comprising a pair of electrodes and a layer of small molecules is shown in Fig. 1a. And Fig. 1b is the scanning electronic microscopic (SEM) image of one storage cell from the direction of a cross-section view. From top to bottom, these layers are the aluminum electrode, **BTVCz–NO$_2$** nanofilm, and ITO glass, respectively. The current–voltage (*I–V*) characteristics of the ITO/**BTVCz–NO$_2$**/Al device are shown in Fig. 1c. In the first sweep from 0 to −4 V, two abrupt current increases were observed at switching threshold voltages around −1.5 V and −2.5 V, indicating that the device underwent sharp electrical transitions from a low-conductivity state ("0" or OFF state) to an intermediate-conductivity state ("1" or ON1 state) and then to a high-conductivity state ("2" or ON2 state). After a subsequent scan from 0 to −4 V, the storage cell remained at its high-conductivity state (sweep 2). Even when a reverse scan from 0 to 4 V was applied, the cell still remained at its high-conductivity state (sweep 3). Sweep 4 was to measure another cell of the device over a voltage range of 0 to −2 V and it showed a switching threshold voltage at −1.5 V. During the subsequent scan from 0 to −4 V, it showed a switching threshold voltage at −2.5 V (sweep 5). This device, therefore, exhibited typical nonvolatile WORM (write-once, read-many-times) memory behaviors.

The transition from "OFF" to "ON1" state and then to "ON2" state can be regarded as the "writing" process for the memory device. It should also be emphasized that our device is highly stable after proper data writing and that a constant voltage (−1.0 V, for example) can be employed to read the "0", "1" and "2" signals of the memory device (Fig. S2a, ESI†). There was no significant degradation in any of the three states for almost ten hours. Furthermore, the effect of continuous read pulses of −1 V on the OFF, ON1 and ON2 states was investigated (Fig. S2b, ESI†). No degradation in the current was observed for

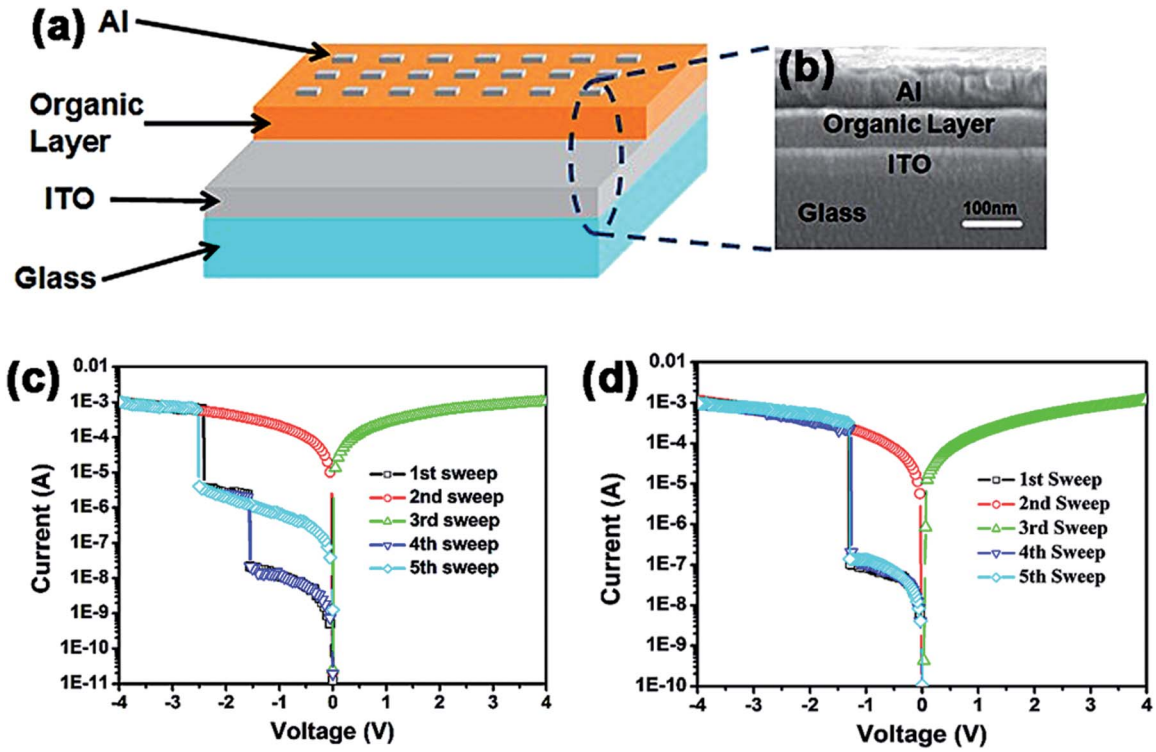

Fig. 1 (a) Illustration of the sandwich device; (b) SEM image of a cross-section view of the device; (c) current–voltage (*I*–*V*) characteristics of the memory device fabricated with the **BTVCz–NO$_2$** film; (d) *I*–*V* characteristics of the memory device fabricated with the **BTVCz** film.

all the three states after more than one hundred million (10^8) continuous read cycles, indicating that any of the states is insensitive to the read pulses.

The three states of the ternary memory cells were very distinct, with the current ratios of "0", "1" and "2" being $\sim 1 : 10^{2.3} : 10^{2.7}$. The switching probability of ITO/**BTVCz–NO$_2$**/Al was 51 out of 64 cells (a device yield of 80%) without encapsulation (Fig. S4, ESI†), which is reasonably acceptable for memory applications.

The ITO/**BTVCz**/Al device showed volatile binary DRAM memory behaviors (Fig. 1d), and its switching threshold voltage was at −1.3 V when an electric field was applied. The DRAM characteristics of the device are testified by the negative voltage scan at the intervals of 0 s, 10 s, 20 s, 30 s, 40 s, 50 s and 60 s, respectively, the OFF current decreased gradually and when the interval time was 60 s the OFF current returned to the original state. The current ratio of "0" and "1" was $10^{3.8}$. The device is also very stable after proper data writing and that a constant voltage (−1.0 V, for example) can be employed to read the "0" and "1" signals of the memory device (Fig. S3a, ESI†). There was no significant degradation in any of the two states for almost ten hours. Herein, the constant voltage means the interval of time is infinitely approximate to 0 s, which is different from the big time gaps in Fig. S6.† Furthermore, the effect of continuous read pulses of −1 V on the OFF and ON states was also investigated (Fig. S3b, ESI†). The stress of voltage of −1 V has a time interval of 2 μs, a very small time gap which is infinitely approximate to 0 in this case. Therefore, no degradation in the current was observed for the two states after more than one hundred million (10^8) continuous read cycles. The switching probability of ITO/**BTVCz**/Al was 55 out of 64 cells (a device yield of 86%) without encapsulation (Fig. S5, ESI†), which is also reasonably acceptable for memory applications in the future.

3.3 Optical properties

As shown in Fig. 2, the UV-vis absorption spectrum of **BTVCz–NO$_2$** in dilute DMF solution displayed a major absorption peak

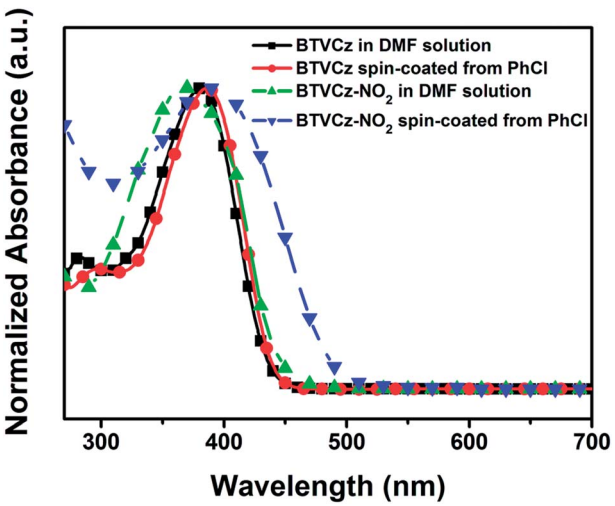

Fig. 2 The UV-vis absorption spectra of **BTVCz–NO$_2$** and **BTVCz** in the DMF solution state and in spin-coated films, respectively.

at 365 nm. We also examined the UV-vis absorption spectrum of the spin-coated **BTVCz–NO$_2$** thin films on ITO substrates. The maximum absorption peak at 400 nm was determined to be 35 nm bathochromic-shifted (from 365 nm to 400 nm) and significantly broadened. In contrast, molecule **BTVCz** in dilute DMF solution exhibited a major absorption peak at 377 nm, whereas its spin-coated film was 8 nm red-shifted and peaked at 385 nm. The red-shift and broadened absorption peaks from solution to solid state might be associated with the formation of molecular aggregation or increased polarizability of the film,[44,45] which is beneficial for improving the charge carrier mobility of the films.

3.4 Electrochemical properties

Fig. 3 shows the cyclic voltammograms (CVs) of two films prepared by spin-coating. The onset oxidations (E_{ox}^{onset}) were 1.06 V and 0.69 V, respectively. The electrochemical potentials were measured using Ag/AgCl as a reference electrode. The external ferrocene/ferrocenium (F_c/F_c^+) redox standard potential (E_{Foc}) was measured to be 0.46 V *vs.* Ag/AgCl in dichloromethane. Assuming that the HOMO level for the F_c/F_c^+ standard is 4.8 eV with respect to the zero vacuum level, the HOMO and LUMO levels for both films are estimated. The detailed results are shown in Table 1.

$$\text{HOMO (eV)} = -[(E_{ox}^{onset}) - E_{Foc} + 4.8] \quad (1)$$

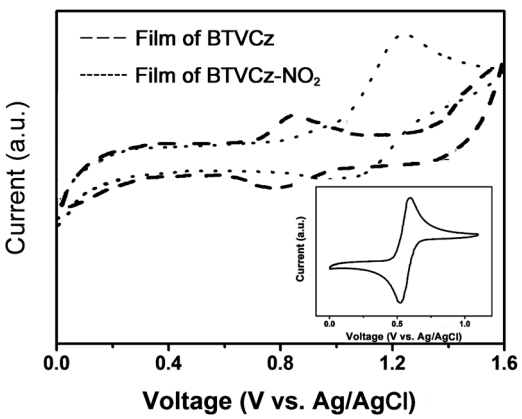

Fig. 3 Cyclic voltammetry (CV) curves of the two films on ITO substrates in dichloromethane with 0.1 mol L^{-1} *n*-Bu_4NPF_6 as the supporting electrolyte and the cyclic voltammetry (CV) curve of the ferrocene standard swept in dichloromethane solution.

$$\text{LUMO (eV)} = \text{HOMO} + E_g \quad (2)$$

$$E_g \text{ (eV)} = 1240/\lambda_{onset} \quad (3)$$

As shown in Table 1, the energy barriers between the work function of the ITO bottom electrode (−4.8 eV) and the HOMO level for the two films were 0.6 eV (**BTVCz–NO$_2$**) and 0.23 eV (**BTVCz**) respectively. And the energy barriers between the LUMO level and the work function of the Al (−4.3 eV) top electrode for the two films were 1.43 eV (**BTVCz–NO$_2$**) and 2.12 eV (**BTVCz**). This finding suggests that hole injection for both films from ITO into the HOMO level is more favorable than electron injection from the Al top electrode into the LUMO level. Thus, both films are p-type materials and hole injection dominates the conduction process.

3.5 Morphology of the thin films

Atomic force microscopy (AFM) was performed to characterize the surface morphology of the two films. As shown in Fig. 4, both films exhibited two-dimensional nanograins in the solid state with uniform size and minor roughness. This type of nanometer-scale grain-like morphology was also observed on other substrates with different polarities, such as glass, silicon oxide, and quartz, indicating that the interaction between the molecules rather than between the molecules and the substrate drives the self-assembly of the molecules. The smooth morphology of these two films facilitates the charge injection from the electrode into the organic molecules. Furthermore, it can prevent the aluminium (Al) electrode from penetrating into the film during the vacuum deposition process. The XRD patterns of films are shown in Fig. 5. The **BTVCz–NO$_2$** film exhibited a conspicuous diffraction peak at $2\theta = 15°$. This value corresponds to a *d*-spacing of 5.9 Å. In contrast, the **BTVCz** film exhibited a diffraction peak at $2\theta = 7.5°$ which equals to a *d*-spacing of 11.8 Å. Therefore, both molecules have good layer-by-layer stacking in their corresponding films.[46–49]

3.6 Proposed data-storage mechanism

To determine the *I–V* performance, the structure of **BTVCz–NO$_2$** was analyzed using density functional theory (DFT) molecular simulations. DFT molecular simulation (Fig. 6a) results show that an open channel is formed from the molecular **BTVCz–NO$_2$** surface throughout the conjugated backbone with continuous positive molecular electrostatic potential (ESP, in red), through

Table 1 Optical and electrochemical properties of BTVCz–NO_2 and BTVCz films

	Film (nm)					
Molecules	λ_{max}	λ_{onset}	E_g^a (eV)	$E_{ox}^{onset b}$ (eV)	HOMO^c (eV)	LUMO (eV)
BTVCz–NO$_2$	400	490	2.53	1.06	5.40	2.87
BTVCz	385	435	2.85	0.69	5.03	2.18

[a] The data were calculated by the following equation: $E_g = 1240/\lambda_{onset}$ of films by two molecules. [b] Against Ag/AgCl in dichloromethane. [c] The HOMO energy levels were calculated from cyclic voltammetry and were referenced to ferrocene (4.8 eV).

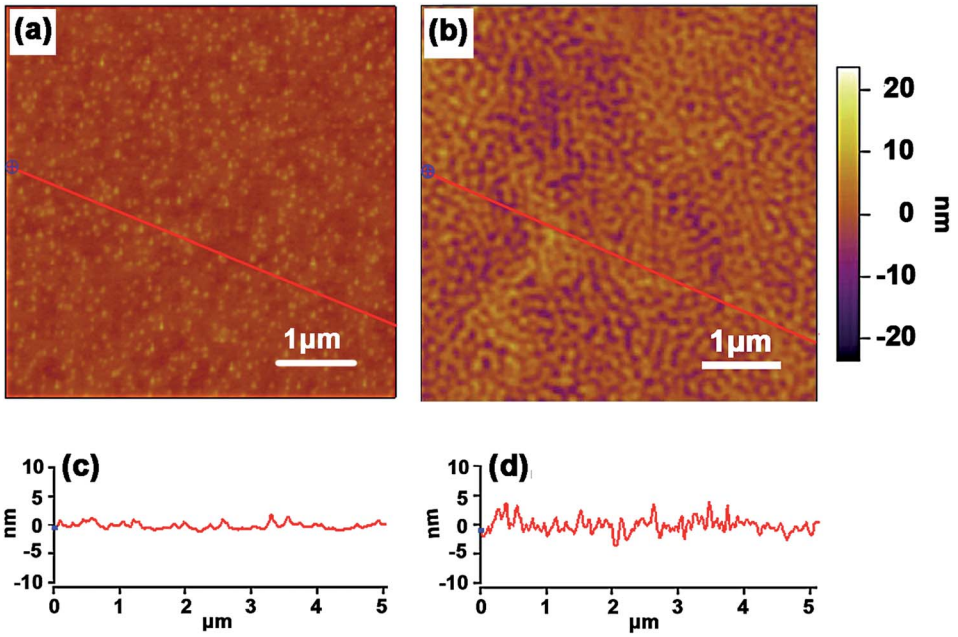

Fig. 4 Tapping-mode AFM height images and typical cross-section profiles of AFM topographic images of two thin films on ITO substrates: (a and c) for molecule **BTVCz–NO$_2$**; (b and d) for molecule **BTVCz**.

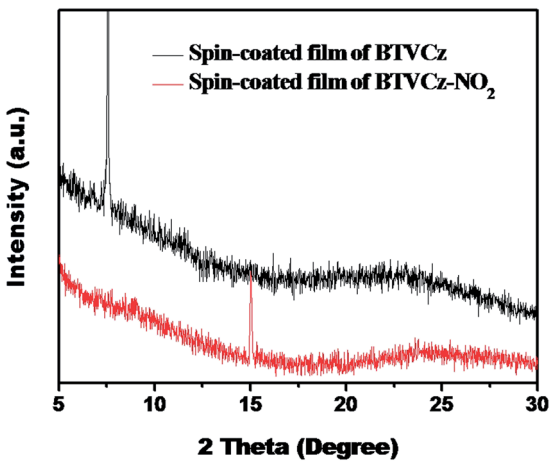

Fig. 5 X-ray diffraction (XRD) scans of two films on the ITO substrate.

which charge carriers can migrate. The negative ESP regions (in blue) caused by the electron-deficient groups, such as nitro chromophores and benzothiazole moieties, can function as "traps" to reduce the mobility of the charge carriers.[50,51] Because of the orderly and close molecular packing, charges transfer among the adjacent molecules easily, and all of the traps have equal opportunities to accept the injected charges. When an electric field is applied, the traps arising from the benzothiazole moiety will be filled up quickly, leading to the current transition from the OFF to the ON1 state. The traps arising from the nitro group will be filled up later, resulting in the current transition from the ON1 to the ON2 state. Upon the HOMO to LUMO transition, the electron density shifts from the donor to the acceptor side and becomes more localized. The nitro group is so deep a trap that the trapped electrons may not be easily detrapped under non-degrading reverse fields, resulting in a high conductivity state that can be maintained for a long time. In sum, the ITO/**BTVCz–NO$_2$**/Al devices show non-volatile ternary WORM-type characteristics.

Whereas only one acceptor (the benzothiazole group) is located in the conjugated molecular backbone as **BTVCz**, therefore, there is only one negative region in the ESP (Fig. 6b) to act as a charge trap to impede the carrier migration, as benzothiazole is a shallow trap. The trap is too shallow to swallow all the charge carriers from the carbazole group and then leads to limited delocalization[52,53] in the carbazole moieties under the electric field. What is more, the studied molecule BTVCz has a weak theoretical dipole moment (3.9 D), which helps in forming the limited delocalization. When the external voltage bias halts, the trapped charge carriers can be de-trapped to the initial states within one minute and the thin film of **BTVCz** returns to a low-conductivity state, thereby DRAM bistable switching behavior is achieved. To clarify how these "traps" can give up the charge carriers after the electric field disappeared, we studied the conduction mechanism of the devices at the "ON" state. After the electrical transition, a linear relationship was observed between $\log(I/V)$ and $V^{1/2}$ in the ITO bottom electrode device (Fig. 6c). This phenomenon follows the Poole–Frenkel emission theory: the "traps" will become much shallower under an electrical field. The change in the depth of "traps" is according to the following formula:[54]

$$\Delta E = \left(q^3/\pi\varepsilon_\theta\varepsilon_0\right)^{\frac{1}{2}}\sqrt{F} \quad (4)$$

where ΔE is the decrement of "traps", q is the charge of an electron, ε_θ is the dielectric constant of the film, ε_0 is the permittivity of free space and F is the electric field intensity.

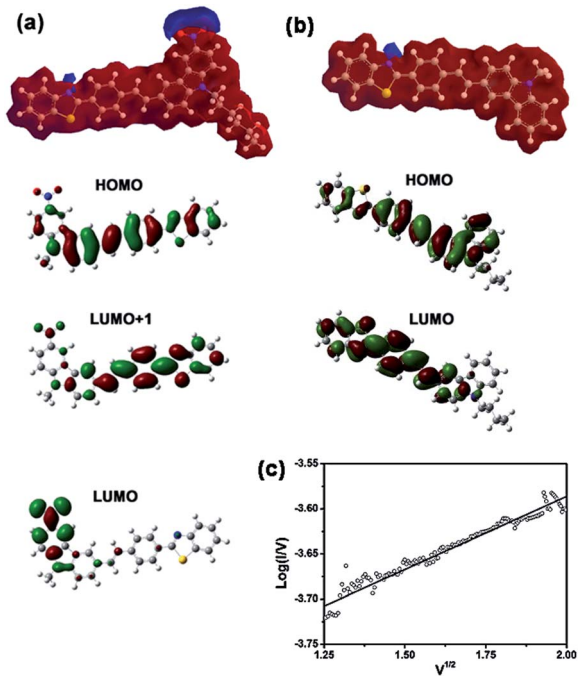

Fig. 6 HOMOs, LUMOs and ESP surfaces of (a) **BTVCz–NO$_2$** and (b) **BTVCz** in their optimized ground-state structures. (c) Linear relationship between log(I/V) and $V^{1/2}$ using ITO as the bottom electrode.

When an electrical field is applied, the injection number of q and the electric field strength (F) increases, leading to a shallower trap depth.

To clarify how the shallow trap discharges when the external bias halts, first of all, we selected a brand-new cell on the device, and then we applied a negative sweep from 0 to −4 V (sweep 1). It was witnessed that the device underwent sharp electrical transitions from the low-conductivity state ("OFF" state) to the high-conductivity state ("ON" state). After that, we applied a negative scan from 0 to −4 V at intervals of 0 s, 10 s, 20 s, 30 s, 40 s, 50 s and 60 s. Here, $\Delta t = 0$ s means that we applied the same sweep from 0 to −4 V. Immediately after sweep 1 it was found that the device was still at its "ON" state. As shown in Fig. S6,† the "OFF" current decreased dramatically in the first several seconds, and then the momentum of its reduction slowed down, but it did not return to its original "OFF" state until $\Delta t = 60$ s when its I–V curve almost overlapped with that of sweep 1. Therefore, the shallow trap arising from the benzothiazole group does not lose all the charge carriers it swallowed before immediately when the external bias halts.

Conclusions

In summary, two organic small molecules, **BTVCz–NO$_2$** and **BTVCz**, were synthesized and fabricated as the electroactive layers of the sandwich-structure memory devices. Both molecules were stacked closely in their spin-coated films with minor fluctuations. The device based on **BTVCz–NO$_2$** films showed nonvolatile ternary WORM data-storage behaviors with switching threshold voltages at −1.5 V and −2.5 V in tandem when an electric field was applied, while its "counterpart" device based on **BTVCz** films exhibited volatile binary DRAM data-storage behaviors with a switching threshold voltage at −1.3 V.

Acknowledgements

This work was financially supported by the Chinese Natural Science Foundation (21176164, 21206102 and 21336005), the NSF of Jiangsu Province (BE2013052), a project of the Department of Education of Jiangsu Province (12KJB430011), Suzhou Nano-project (ZXG2012023) and the Project supported by the Specialized Research Fund for the Doctoral Program of Higher Education of China (Grant no. 20113201130003 and 20123201120005).

Notes and references

1 J. Lee, E. Lee, S. Kim, G. S. Bang, D. A. Shultz, R. D. Schmidt, M. D. E. Forbes and H. Lee, *Angew. Chem., Int. Ed.*, 2011, **50**, 4414–4418.
2 J. S. Lee, *J. Mater. Chem.*, 2011, **21**, 14097–14112.
3 J. C. Scott and L. D. Bozano, *Adv. Mater.*, 2007, **19**, 1452–1463.
4 N. H. You, C. C. Chueh, C. L. Liu, M. Ueda and W. Chen, *Macromolecules*, 2009, **42**, 4456–4463.
5 D. I. Son, T. W. Kim, J. H. Shim, J. H. Jung, D. U. Lee, J. M. Lee, W. I. Park and W. K. Choi, *Nano Lett.*, 2010, **10**, 2441–2447.
6 C. W. Chu, J. Ouyang, J. H. Tseng and Y. Yang, *Adv. Mater.*, 2005, **17**, 1440–1443.
7 Q. D. Ling, D. J. Liaw, C. Zhu, D. S. H. Chan, E. T. Kang and K. G. Neoh, *Prog. Polym. Sci.*, 2008, **33**, 917–978.
8 E. Kapetanakis, A. Douvas, D. Velessiotis, E. Makarona, P. Argitis, N. Glezos and P. Normand, *Adv. Mater.*, 2008, **20**, 4568–4574.
9 J. Ouyang, C. Chu, C. Szmanda, L. Ma and Y. Yang, *Nat. Mater.*, 2004, **3**, 918–922.
10 C. Ye, Q. Peng, M. Li, J. Luo, Z. Tang, J. Pei, J. Chen, Z. Shuai, L. Jiang and Y. Song, *J. Am. Chem. Soc.*, 2012, **134**, 20053–20059.
11 Y. Ma, Y. Wen, J. Wang, Y. Shang, S. Du, L. Pan, G. Li, L. Yang, H. Cao and Y. Song, *J. Phys. Chem. C*, 2009, **113**, 8548–8552.
12 Y. Shang, Y. Wen, S. Li, S. Du, X. He, L. Cai, Y. Li, L. Yang, H. Gao and Y. Song, *J. Am. Chem. Soc.*, 2007, **129**, 11674–11675.
13 G. Li, K. Zheng, C. Wang, K. Leck, F. Hu, X. Sun and Q. Zhang, *ACS Appl. Mater. Interfaces*, 2013, **5**, 6458–6462.
14 P. Gu, F. Zhou, J. Gao, G. Li, C. Wang, Q. Xu, Q. Zhang and J. Lu, *J. Am. Chem. Soc.*, 2013, **135**, 14086–14089.
15 R. Naber, K. Asadi, P. Blom, D. de Leeuw and B. de Boer, *Adv. Mater.*, 2010, **22**, 933–945.
16 J. C. Scott, *Science*, 2004, **304**, 62–63.
17 K. Kim, Y.-K. Fang, W. Kwon, S. Pyo, W.-C. Chen and M. Ree, *J. Mater. Chem. C*, 2013, **1**, 4858–4868.
18 C.-J. Chen, H.-J. Yen, Y.-C. Hu and G.-S. Liou, *J. Mater. Chem. C*, 2013, **1**, 7623–7634.

19 S. Park, K. Kim, D. M. Kim, W. Kwon, J. Choi and M. Ree, *ACS Appl. Mater. Interfaces*, 2011, **3**, 765–773.
20 S. G. Hahm, S. Choi, S.-H. Hong, T. J. Lee, S. Park, D. M. Kim, J. C. Kim, W. Kwon, K. Kim, M.-J. Kim, O. Kim and M. Ree, *J. Mater. Chem.*, 2009, **19**, 2207–2214.
21 T. J. Lee, Y.-G. Ko, H.-J. Yen, K. Kim, D. M. Kim, W. Kwon, S. G. Hahm, G.-S. Liou and M. Ree, *Polym. Chem.*, 2012, **3**, 1276–1283.
22 W. Kwon, B. Ahn, D. M. Kim, Y.-G. Ko, S. G. Hahm, Y. Kim, H. Kim and M. Ree, *J. Phys. Chem. C*, 2011, **115**, 19355–19363.
23 Y.-H. Chou, H.-J. Yen, C.-L. Tsai, W.-Y. Lee, G.-S. Liou and W.-C. Chen, *J. Mater. Chem. C*, 2013, **1**, 3235.
24 L.-H. Xie, Q.-D. Ling, X.-Y. Hou and W. Huang, *J. Am. Chem. Soc.*, 2008, **130**, 2120–2121.
25 C.-J. Chen, H.-J. Yen, W.-C. Chen and G.-S. Liou, *J. Mater. Chem.*, 2012, **22**, 14085–14093.
26 Y. Lai, K. Ohshimizu, W. Lee, J. Hsu, T. Higashihara, M. Ueda and W.-C. Chen, *J. Mater. Chem.*, 2011, **21**, 14502–14508.
27 J. Liu, Z. Yin, X. Cao, F. Zhao, A. Lin, L. Xie, Q. Fan, F. Boey, H. Zhang and W. Huang, *ACS Nano*, 2010, **4**, 3987–3992.
28 Q. D. Ling, F. C. Chang, Y. Song, C. X. Zhu, D. J. Liaw, D. S. H. Chan, E. T. Kang and K. G. Neoh, *J. Am. Chem. Soc.*, 2006, **128**, 8732–8733.
29 Y. Z. Lin, Y. F. Li and X. W. Zhan, *Chem. Soc. Rev.*, 2012, **41**, 4245–4272.
30 K. B. Burke, Y. Shu, P. Kemppinen, B. Singh, M. Bown, I. I. Liaw, R. M. Williamson, L. Thomsen, P. Dastoor, W. Belcher, C. Forsyth, K. N. Winzenberg and G. E. Collis, *Cryst. Growth Des.*, 2012, **12**, 725–731.
31 Q. Q. Shi, P. Cheng, Y. F. Li and X. W. Zhan, *Adv. Energy Mater.*, 2012, **2**, 63–67.
32 A. W. Hains, Z. Liang, M. A. Woodhouse and B. A. Gregg, *Chem. Rev.*, 2010, **110**, 6689–6735.
33 B. Walker, C. Kim and T. Q. Nguyen, *Chem. Mater.*, 2011, **23**, 470–482.
34 Y. Li, Q. Guo, Z. Li, J. Pei and W. Tian, *Energy Environ. Sci.*, 2010, **3**, 1427–1436.
35 J. Roncali, *Acc. Chem. Res.*, 2009, **42**, 1719–1730.
36 H. X. Shang, H. J. Fan, Y. Liu, W. P. Hu, Y. F. Li and X. W. Zhan, *Adv. Mater.*, 2011, **23**, 1554–1557.
37 H. Li, Q. Xu, N. Li, R. Sun, J. Ge, J. Lu, H. Gu and F. Yan, *J. Am. Chem. Soc.*, 2010, **132**, 5542–5543.
38 S. Miao, H. Li, Q. Xu, N. Li, J. Zheng, R. Sun, J. Lu and C. M. Li, *J. Mater. Chem.*, 2012, **22**, 16582–16589.
39 S. Miao, H. Li, Q. Xu, Y. Li, S. Ji, N. Li, L. Wang, J. Zheng and J. Lu, *Adv. Mater.*, 2012, **24**, 6210–6215.
40 B. Lei, W. L. Kwan, Y. Shao and Y. Yang, *Org. Electron.*, 2009, **10**, 1048–1053.
41 W.-J. Joo, T.-L. Choi, J. Lee, S. K. Lee, M.-S. Jung, N. Kim and J. M. Kim, *J. Phys. Chem. B*, 2006, **110**, 23812–23816.
42 J. Lin and D. Ma, *Appl. Phys. Lett.*, 2008, **93**, 093505.
43 H. Wang, G. Chen, X. Xu, H. Chen and S. Ji, *Dyes Pigm.*, 2010, **86**, 238–248.
44 M. Surin, P. Sonar, A. C. Grimsdale, K. Müllen, S. De Feyter, S. Habuchi, S. Sarzi, E. Braeken, A. V. Heyen, M. Van Der Auweraer, F. C. De Schryver, M. Cavallini, J. F. Moulin, F. Biscarini, C. Femoni, L. Roberto and P. Leclère, *J. Mater. Chem.*, 2007, **17**, 728–735.
45 R. Schmidt, J. H. Oh, Y.-S. Sun, M. Deppisch, A.-M. Krause, K. Radacki, H. Braunschweig, M. Könemann, P. Erk, Z. Bao and F. Würthner, *J. Am. Chem. Soc.*, 2009, **131**, 6215–6228.
46 S. Loser, C. Bruns, H. Miyauchi, R. Ortiz, A. Facchetti, S. Stupp and T. Marks, *J. Am. Chem. Soc.*, 2011, **133**, 8142–8145.
47 L. Li, P. Gao, K. Schuermann, S. Ostendorp, W. Wang, C. Du, Y. Lei, H. Fuchs, L. De Cola, K. Müllen and L. Chi, *J. Am. Chem. Soc.*, 2010, **132**, 8807–8809.
48 T. Chen, X. Wu and R. Rieke, *J. Am. Chem. Soc.*, 1995, **117**, 233–244.
49 T. Prosa, M. Winokur, J. Moulton, P. Smith and A. Heeger, *Macromolecules*, 1992, **25**, 4364–4372.
50 X.-D. Zhuang, Y. Chen, G. Liu, B. Zhang, K.-G. Neoh, E.-T. Kang, C.-X. Zhu, Y.-X. Li and L.-J. Niu, *Adv. Funct. Mater.*, 2010, **20**, 2916–2922.
51 G. Liu, B. Zhang, Y. Chen, C.-X. Zhu, L. Zeng, D. S.-H. Chan, K.-G. Neoh, J. Che and E.-T. Kang, *J. Mater. Chem.*, 2011, **21**, 6027–6033.
52 Q. Ling, Y. Song, S. Lim, E. Teo, Y. Tan, C. Zhu, D. Chan, D. Kwong, E. Kang and K. Neoh, *Angew. Chem.*, 2006, **118**, 3013–3017.
53 Y. Fang, C. Liu, G. Yang, P. Chen and W. Chen, *Macromolecules*, 2011, **44**, 2604–2612.
54 G. Ottaviani, C. Canali, C. Jacoboni and A. Quaranta, *J. Appl. Phys.*, 1973, **44**, 360.

